UNCLASSIFIED
SECURITY CLASSIFICATION OF THIS PAGE

AD-A206 259

REPORT DOCUMENTATION PAGE

Form Approved
OMB No. 0704-0188

1a. REPORT SECURITY CLASSIFICATION UNCLASSIFIED	1b. RESTRICTIVE MARKINGS
2a. SECURITY CLASSIFICATION AUTHORITY	3. DISTRIBUTION/AVAILABILITY OF REPORT Approved for public release; distribution is unlimited.
2b. DECLASSIFICATION/DOWNGRADING SCHEDULE	
4. PERFORMING ORGANIZATION REPORT NUMBER(S) ARL-TR-89-2	5. MONITORING ORGANIZATION REPORT NUMBER(S)
6a. NAME OF PERFORMING ORGANIZATION Applied Research Laboratories 6b. OFFICE SYMBOL (If applicable) ARL:UT	7a. NAME OF MONITORING ORGANIZATION Office of the Chief of Naval Research
6c. ADDRESS (City, State, and ZIP Code) The University of Texas at Austin P.O. Box 8029 Austin, Texas 78713-8029	7b. ADDRESS (City, State, and ZIP Code) Department of the Navy Arlington, Virginia 22217-5000
8a. NAME OF FUNDING/SPONSORING ORGANIZATION 8b. OFFICE SYMBOL (If applicable)	9. PROCUREMENT INSTRUMENT IDENTIFICATION NUMBER N00014-84-K-0082
8c. ADDRESS (City, State, and ZIP Code)	10. SOURCE OF FUNDING NUMBERS PROGRAM ELEMENT NO. / PROJECT NO. / TASK NO. / WORK UNIT ACCESSION NO.

11. TITLE (Include Security Classification)

Acoustic Echo Degradation of Small Targets Buried in Sediment: A Theoretical Study

12. PERSONAL AUTHOR(S)
Nicholas P. Chotiros

13a. TYPE OF REPORT	13b. TIME COVERED	14. DATE OF REPORT (Year, Month, Day)	15. PAGE COUNT
technical	FROM _____ TO _____	89-1-10	36

16 SUPPLEMENTARY NOTATION

17. COSATI CODES		
FIELD	GROUP	SUB-GROUP

18. SUBJECT TERMS (Continue on reverse if necessary and identify by block number)
acoustic scattering; Shallow grazing angle;
bottom penetration; Backscattering;
buried target detection. (edc)

19. ABSTRACT (Continue on reverse if necessary and identify by block number)

The behavior of a small target in two representative types of sediment was examined. The two types of sediment considered were a soft silty sediment whose sound velocity is slightly less than that of water and a sandy sediment with a much higher sound velocity. The reduction in the target echo due to the presence of the sediment was quantified as a "sediment factor". The sediment factor was examined both qualitatively and quantitatively. Qualitatively, it was found that an acoustic field may be divided into distinct zones. For quantitative results, computer simulations, using the SAFARI full wave mathematical model, were used to obtain numerical estimates of the sediment factor. In general, the sediment factor due to the presence of the sediment was found to be more complicated than expected. The results obtained in this report are based entirely on computer models and they remain to be verified by an experiment. Keywords;

20. DISTRIBUTION/AVAILABILITY OF ABSTRACT	21. ABSTRACT SECURITY CLASSIFICATION
☐ UNCLASSIFIED/UNLIMITED ☒ SAME AS RPT. ☐ DTIC USERS	UNCLASSIFIED
22a. NAME OF RESPONSIBLE INDIVIDUAL Nicholas P. Chotiros	22b. TELEPHONE (Include Area Code) 512-835-3512 / 22c. OFFICE SYMBOL ASG

DD Form 1473, JUN 86 — Previous editions are obsolete. — SECURITY CLASSIFICATION OF THIS PAGE

UNCLASSIFIED

TABLE OF CONTENTS

Page

LIST OF FIGURES

LIST OF TABLES

ACKNOWLEDGMENTS

Thanks are due to the SACLANT Research Centre for the use of the SAFARI program, to Robert Koch and Jay Scott for assistance with the SAFARI program, and to Evan Westwood for the complex ray model. The computer runs on the SAFARI program were ably executed by Tim Hoar on the ARL:UT Alliant computer, and on the complex ray model by Robert Altenburg on the ARL:UT CYBER 830. I also want to thank several people for information and useful discussions: John Huckabay, Robert Culbertson, Morrie Stern, and Larry Satkowiak of NCSC, Panama City, Florida. Thanks are due to Robert Obrochta and the Office of the Chief of Naval Research for support and encouragement.

1. INTRODUCTION

This work has been a theoretical study of the process of acoustic scattering from small objects at the water-sediment interface or buried in the sediment. An object is regarded as "small" if its dimensions are small compared to the acoustic wavelengths in the frequency band of interest. At normal incidence, acoustic scattering from these objects is a fairly simple problem, which has been analyzed in connection with depth sounder applications. Our study is aimed at the shallow grazing angle case, which is particularly relevant to detection applications. In particular, we would like to obtain estimates of the degradation in the acoustic backscatter of the buried objects. We will consider acoustic frequencies less than 1 kHz such that the acoustic wavelength will be large compared to objects of about a meter in size.

This report is divided into five main sections: In Section 2, the theoretical tools will be described. Both the physical models and the systems parameters will be described. In Section 3, the application of reciprocity to estimate the backscattered signal is described. In Section 4, the resulting theoretical model is applied to specific cases. The results and conclusions are summarized in Section 5.

2. THEORY

The theoretical considerations may be divided into two main complementary parts, physical processes and systems analysis. The former concerns the sound propagation and scattering models and the latter concerns the system parameters, particularly the degradation in target echo.

2.1 PHYSICAL PROCESSES

We require a theoretical model that can accurately predict the propagation of sound waves through the water, through the water/sediment interface, the interaction of the sound waves with a small object, and the backscattered signal from the object back to the point of transmission. Analytical solutions are only practical for plane wave problems with one interface. Clearly, this will not be adequate for studying the backscatter of sound from small objects, particularly in cases where the object is near or at the interface, or where the medium is multilayered. Therefore it was decided to approach the problem through numerical computer simulations.

Objects may become buried in sediment through a variety of mechanisms, including sedimentation of waterborne material or scouring of the surrounding material; or, the object may simply sink into a soft sediment under its own weight. This type of burial implies either sand or silt sediments, and thus the study will be limited to these two types of sediments. The detection of objects that are embedded in solid rock sediment will not be considered.

Sand and silt sediments are porous solid media. The theory of sound propagation in porous media was first developed by Biot [1-5] The porous solid differs from the viscoelastic solid in that it can support two longitudinal waves, a fast wave and a slow wave. The fast wave corresponds to the acoustic wave in a viscoelastic solid, but the slow wave has no counterpart in a viscoelastic solid. Stern[6] has developed a numerical model for a horizontally stratified porous medium, but it only deals with plane waves; and Norris[7] has published a theoretical model for radiation and scattering of sound in a homogeneous porous medium. Thus, it appears that most of the components for producing a

propagation model in porous media are available, but they have not yet been assembled in a comprehensive package.

The principal difference between a porous solid and a viscoelastic one is the presence of the slow wave. Stern[6] has shown that the slow wave velocity is frequency dependent. From his results, it appears that for frequencies below 1 kHz, the slow wave velocity is too low to have any significant effect on the sound field, and thus the sediment may be approximated as a viscoelastic solid. Therefore, it is not imperative that we use the Biot model for porous media. Since mathematical models for viscoelastic solids already exist in very comprehensive packages, we have chosen to approximate the sediment as a viscoelastic solid.

For computer simulation of sound propagation in viscoelastic media, the finite difference[8] and finite element[9] methods are the most general methods but their computation resource requirements are prohibitive. The parabolic equation method[10] is inadequate because it ignores shear stress and strain. Ray tracing methods[11] are also inadequate because they are only high frequency approximations and are expected to be particularly inaccurate in the vicinity of the interfaces.

Of the computer models that are currently available, the seismic and acoustic fast-field-program for range independent environments (SAFARI) model, developed at the SACLANT Research Centre by Schmidt and Jensen,[12,13] is the most complete. It gives a full wave solution for the field generated by a point source, in a horizontally stratified viscoelastic medium. This is done by decomposing the acoustic field from a point source into a series of plane waves, and then solving the field solutions for all plane wave components and superimposing them to give the total field. The algorithm is an integral part of the signal processing package that can simulate the propagation of an arbitrary signal projected from an arbitrary array of point sources. Therefore the SAFARI model will be our main model for quantitative analyses.

For a qualitative look at the acoustic pressure field, the complex ray model[14] is very efficient. It is particularly efficient when applied to Gaussian beams. Results from the complex ray model have been successfully compared

with the results of the full wave methods in bench mark tests. In comparisons with the SAFARI model, significant quantitative differences were found but, qualitatively, their results were very similar. That is, the two models showed similar acoustic pressure amplitude distributions, but there were differences in the absolute levels. The complex ray model only takes a small fraction of the computation time that SAFARI takes. The computation time requirement of the complex ray model is relatively insensitive to the angle of incidence, while that of the SAFARI model increases rapidly with grazing angle. In fact, it is simply not practical to use the SAFARI for near-normal incidence angles. Therefore, the complex ray model will be used as a qualitative support.

The main deficiency in the SAFARI model is the constraint of a horizontally stratified medium. This means that SAFARI cannot directly model the signal scattered from a small object. It may be used to predict the propagation loss to and from the object, but the scattering strength of the object itself must be computed separately.

There are very few experimental verifications of the SAFARI model. An experiment has been conducted recently by Satkowiak,[15] Naval Coastal Systems Center (NCSC), in cooperation with the Admiralty Research Establishment (ARE), U.K., at the ARE facility in Portland, U.K. Experiments conducted by Applied Research Laboratories, The University of Texas at Austin (ARL:UT) in cooperation with other Navy laboratories, off Kings Bay, Georgia, and in cooperation with NCSC, off Panama City, gave mixed results. These were high frequency acoustic experiments, in the region of 10-100 kHz, where the slow wave velocity is such that significant coupling may occur. For the frequency range of interest, that is, less than 1 kHz, as far as we know, the viscoelastic solid approximation is valid.

2.2 SYSTEMS ANALYSIS

Let us start with the sonar equation. As illustrated in Fig. 2.1, the signal S_{to} returned by a object of target strength T_S at a range r in an unbounded body of water is given by

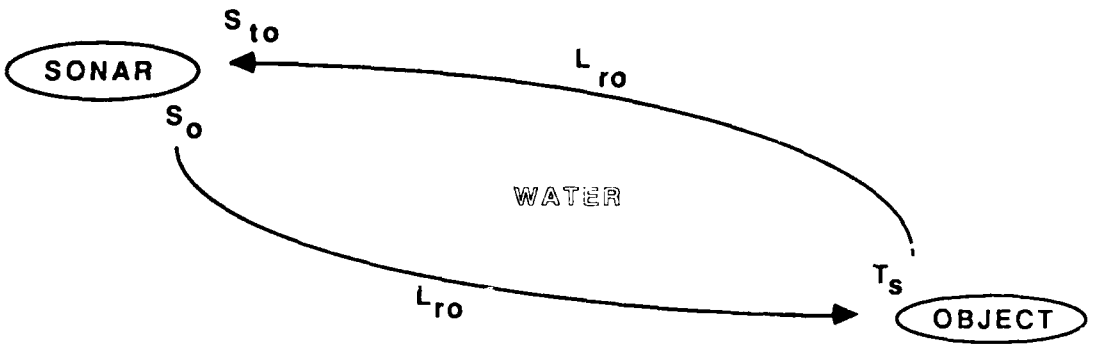

(a) DETECTION IN WATER

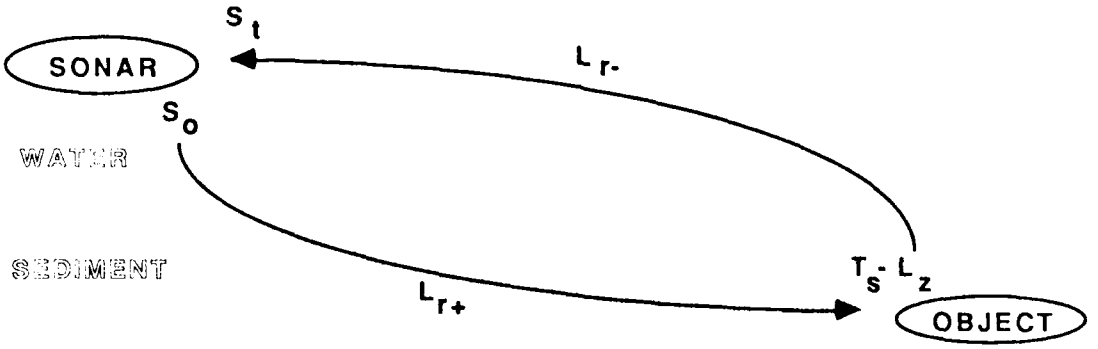

(b) DETECTION IN SEDIMENT

FIGURE 2.1

SYSTEM PARAMETERS FOR TARGET DETECTION

ARL - UT
AS-89-9
NPC - RFO
1 - 20 - 89

$$S_{to} = S_o + T_s - L_{2ro} \quad , \tag{2-1}$$

where S_o is the source level and L_{2ro} is the two-way propagation loss in water at the range r. For both source and target in a homogeneous medium, the two-way propagation loss is simply twice the one way loss L_{ro},

$$L_{2ro} = 2\, L_{ro} \quad . \tag{2-2}$$

Let us use the above equations as our standard against which the return from small targets at the sediment interface or buried within the sediment will be compared. With reference to Fig. 2.1, the return S_t from the same target at the interface or within the sediment is given by

$$S_t = S_o + T_s - L_{2r} \quad , \tag{2-3}$$

where L_{2r} is the effective two-way propagation loss.

Our objective is to estimate the change in signal level due to the presence of the sediment, which we will call the "sediment factor" F_s, defined as

$$F_s = S_t - S_{to}$$

$$= L_{2r} - L_{2ro} \quad . \tag{2-4}$$

It is a quantitative measure of the signal degradation caused by the presence of the sediment.

Let us examine L_{2r}, the main constituent of the sediment factor, more closely. It is implied in the above equations that the target strength T_s is the target strength as measured in water. If the object were placed in the sediment, then its target strength will undergo a change L_z. It is also possible that the pressure propagation loss along the outward bound path L_{r+} may not be equal to that of the return path L_{r-}. The effective two-way propagation loss may be defined as the sum of these three components,

$$L_{2r} = L_{r+} + L_{r-} + L_z \quad . \tag{2-5}$$

Due to the complicated nature of the propagation process, we will rely on computer simulations to give the quantitative estimates of L_{r+}. Assuming that return paths are simply the reverse of the outward bound paths, it is possible to estimate the propagation loss difference $L_{r-} - L_{r+}$ by reciprocity and the target loss L_z from the sediment properties.

3. THE BACKSCATTERED SIGNAL

3.1 TARGET STRENGTH

The target strength of small objects are of immediate interest. Target strength T_S in decibels is defined in terms of the acoustic cross section σ by

$$T_S = 10 \log_{10}(\sigma/4\pi) \quad . \tag{3-1}$$

For a solid sphere that is small compared to the wavelength, the acoustic cross section derived by Rayleigh[16] and later by Anderson[17] is given by

$$\sigma_{sphere} = 4\pi a^2 (ka)^4 R \quad , \tag{3-2}$$

where k is the acoustic wave number in the surrounding medium and a is the radius; R is a constant dependent on material properties,

$$R = [(1-gh^2)/(3gh^2) + (1-g)/(1+2g)]^2 \quad , \tag{3-3}$$

where h and g are the sound velocity and density ratios between the sphere and the surrounding medium.

Let us examine a few asymptotic cases: consider the cases where the values of g (velocity ratio) and h (density ratio) are either 0, 1, or infinite. The resulting values of R for all reasonable combinations is given in the table below. Certain combinations, such as $h=\infty$ and g=0, are not reasonable since they do not yield deterministic results and do not approximate any object constructed of real materials.

TABLE 3.1
ASYMPTOTIC VALUES OF R

g	h	R	Remarks
0	0	∞	Trapped gas bubbles
1	1	0	Undetectable object
1	∞	0.33	Very rigid object of same density as medium
∞	1	0.69	Very dense object of same sound velocity as the medium
∞	∞	0.69	Very rigid and very dense object

It is interesting to note that a low rigidity and low density object will have a very large value of R, indicating that trapped gas bubbles may be very strong sound scatterers. An object with the same density and sound speed as the medium will not be detectable. In water, silt, or sand, there is a large class of man-made objects that can be considered as being either very much more dense or very much more rigid than the medium. It can be seen that such targets will have R values between 0.33 and 0.69.

Rewriting Eq. (3-2) in terms of volume, we get

$$\sigma_{sphere} = (9/4\pi)\, V^2\, k^4\, R \quad , \tag{3-4}$$

where V is the volume of the sphere.

It is expected a similar expression would be applicable for objects that are very small compared to the wavelength. It is known, for example, that for any dense and rigid elongated solid of revolution,[18] the acoustic cross section in the axial direction is independent of shape, given by

$$\sigma_{rigid\ dense\ elongated} = (4/\pi)\, V^2\, k^4 \quad , \tag{3-5}$$

where V is the volume of the object.

It is seen that Eqs. (3-4) and (3-5) are of the same form, differing only in the values of the constant multiplier.

Therefore, the acoustic backscattering cross section of small objects can be expected to vary as

$$\sigma = C V^2 k^4 \quad , \tag{3-6}$$

where the constant C is weakly dependent on the shape and orientation of the object.

It is seen that target strength is proportional to the fourth power of the speed of sound in the surrounding medium. Therefore, the change in target strength incurred by moving a target from one medium into another is simply given by the fourth power of the sound velocity ratio,

$$L_Z = -40 \log_{10}(r_C) \quad , \tag{3-7}$$

where r_C is the sound velocity in the second medium divided by the sound velocity in the first medium.

3.2 RECIPROCITY

All of the above models assume that the medium is linear. Therefore the signal path between source and receiver may be considered as a linear network. From linear network theory, it is known that the forward and reverse paths must satisfy the reciprocity theorem. In this context, the reciprocity theorem may be interpreted as follows: If a source at a position A, defined in terms of volume displacement, produces a certain level of pressure at a position B, then a source of equal strength at B will produce the same pressure at A.

Both the SAFARI and complex ray models estimate the pressure propagation at any point B produced by a unit pressure source at A, where the source level is defined in terms of pressure at a reference radial distance of 1 m. Therefore the pressures at A and B produced by unit sources at B and A,

respectively, are expected to differ by a factor equal to the ratio of the acoustic impedances at the two points. Therefore the propagation loss difference is given by

$$L_{r-} - L_{r+} = 20 \log_{10}(r_z) \quad , \tag{3-8}$$

where r_z is the local acoustic impedance at the target position divided by that at the source position.

The acoustic impedance in an homogeneous medium is equal to the product of the density and the sound speed. This is also approximately true in a layered medium for points several wavelengths away from the discontinuities. For points near or on a boundary between two layers, the impedance is not easily determined, but it is expected to have an intermediate value. Thus, let us approximate the effective impedance Z, at a point in a medium with impedance Z_1 at a distance d from the interface with a medium of impedance Z_2, by

$$Z = (Z_1 e^{-d/\lambda_1} + Z_2)/(e^{-d/\lambda_1} + 1) \quad , \tag{3-9}$$

where λ_1 is the wavelength in the medium with impedance Z_1.

4. COMPUTER SIMULATIONS

4.1 SEDIMENT PROPERTIES

As stated earlier, the study is limited to sediments that may be described as either silt or sand, or some combination thereof. For practical purposes, let us restrict the study to the first 100 m of the sediment. Over such a short depth interval, there is usually very little change in the sediment properties, and therefore they may be regarded as constant. A set of typical values[19-23] of the properties of silt and sand in the upper 100 m is shown in Table 4.1. These values will be used in the numerical models to compute the sediment factor of signals backscattered by a small object. In these simulations, the sonar is positioned at a height of 100 m above the sediment interface. The sound velocity and density of the water are assumed to be 1540 m/s and 1000 kg/m^3, respectively.

TABLE 4.1
TYPICAL SEDIMENT PROPERTIES

Silt sediment		
Density	1400	kg/m^3
Sound velocity	1500	m/s
Sound velocity gradient	1	s^{-1}
Sound absorption coefficient	0.5	dB/λ
Shear wave velocity	0	m/s
Shear absorption coefficient	-	dB/λ
Sand sediment		
Density	2000	kg/m^3
Sound velocity	1725	m/s
Sound velocity gradient	0	s^{-1}
Sound absorption coefficient	0.5	dB/λ
Shear wave velocity	55	m/s
Shear absorption coefficient	3.44	dB/λ

4.2 ACOUSTIC PRESSURE FIELD

In a water logged silt sediment, the sound velocity is almost identical to that of the water. In gassy silt sediments, the sound velocities are often less than that of water. In these sediments, sound propagates directly into the sediment by refraction and with very little loss. There is a critical angle in the sediment which forces the refracted waves to emerge at incidence angles less than or equal to the critical angle. Beyond a corresponding critical range, this effect becomes dominant. There is the possibility of interference effects between the sound waves from the two sides of the critical range, as illustrated in Fig. 4.1. Thus, the acoustic field may be considered in terms of three zones, the refraction, critical refraction, and interference zones.

In a compacted sand sediment, the sound velocity is significantly higher than that of water. Acoustic energy may be introduced into the sediment by two mechanisms, refraction and tunneling. Near normal incidence, sound waves are refracted into the sediment in the usual way. At the critical angle, the sound energy is refracted in a direction that is almost parallel to the interface. For incidence angles greater than the critical angle, there is total reflection. Thus, beyond a corresponding critical range, sound may not enter the sediment by refraction. Instead, it enters as an evanescent wave that tunnels into the sediment to a depth of a few wavelengths. Since the refracted and evanescent waves travel at different velocities they are expected to produce an interference pattern. Thus, the acoustic field may be considered in terms of three zones, the refraction, the evanescent, and the interference zones, as shown in Fig. 4.2.

A numerical example of the sound pressure contours for a sandy sediment, computed by the complex ray model, is shown in Fig. 4.3. It shows the in-sediment constant pressure amplitude contours produced by a unit point source 100 m above the sediment operating at 100 Hz. The critical angle is calculated to be 63.2°; the critical ray intersects the interface at a horizontal distance of 198 m. It is seen that for ranges greater than about 200 m, the sound field appears to be divisible into three distinct regions. Nearest the interface, there is a region where the contours of constant sound pressure are nearly horizontal and very tightly packed, indicative of the rapid decay rate of the evanescent pressure with depth. Farthest from the interface, there is a

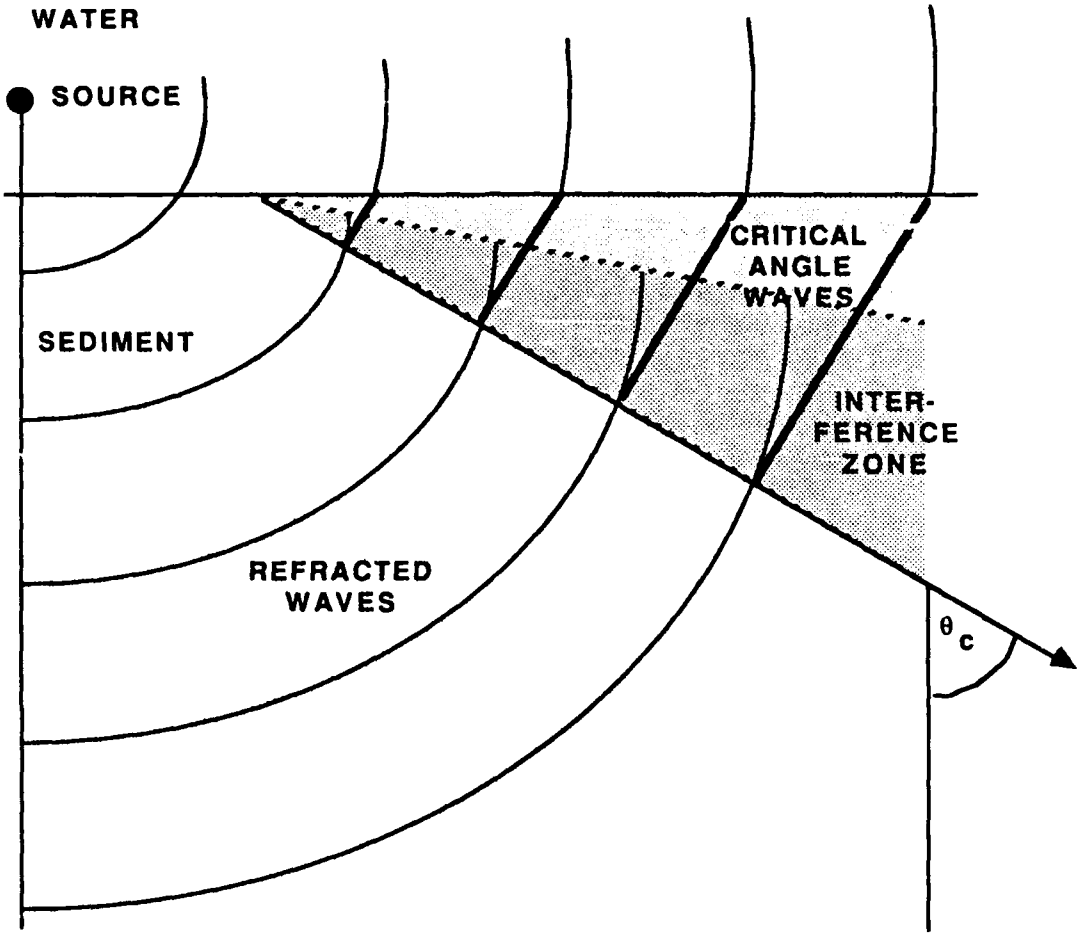

FIGURE 4.1

SOUND PROPAGATION FROM WATER INTO A SILTY SEDIMENT

ARL - UT
AS-89-10
NPC - RFO
1 - 20 - 89

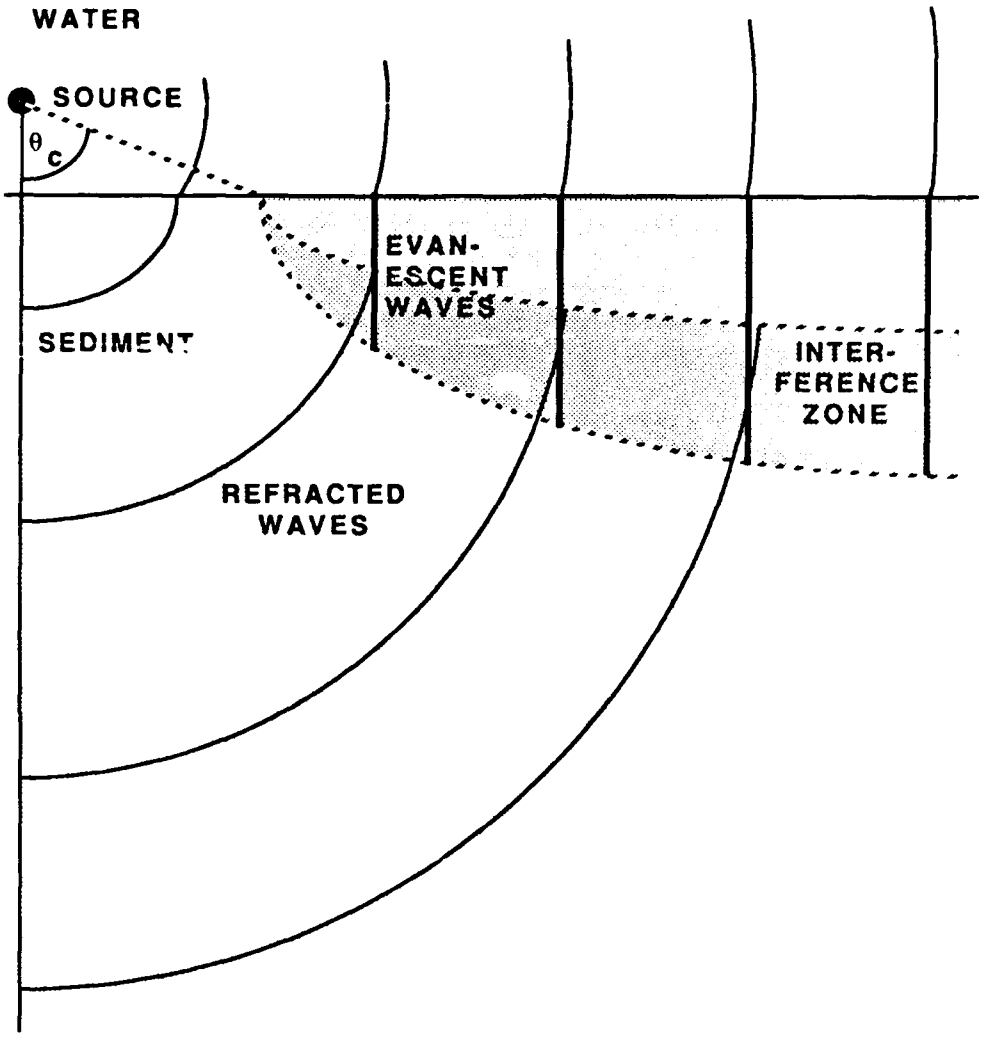

FIGURE 4.2

SOUND PROPAGATION FROM WATER INTO A SANDY SEDIMENT

ARL - UT
AS-89-11
NPC - RFO
1 - 20 - 89

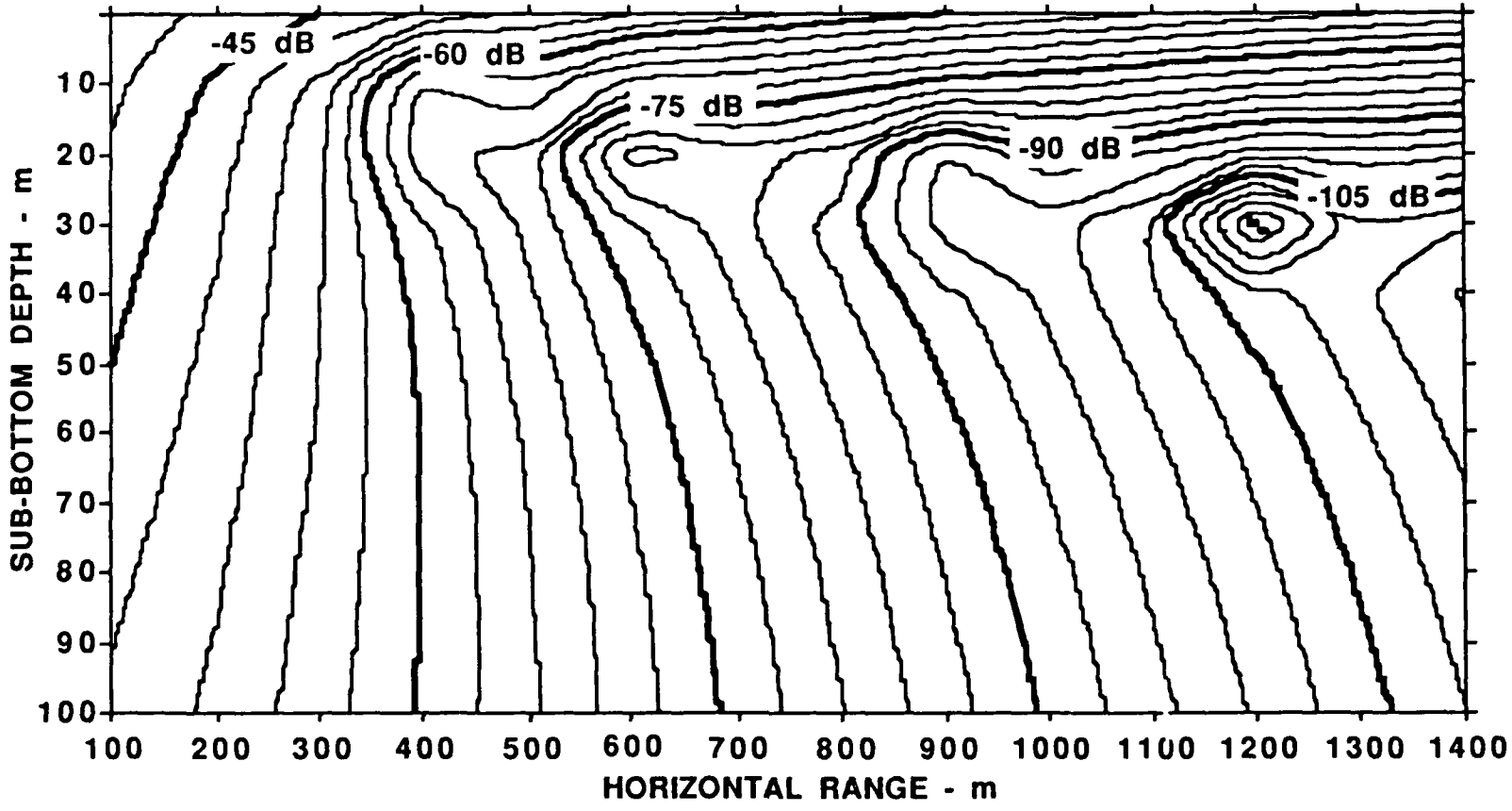

FIGURE 4.3
APPROXIMATE PRESSURE CONTOURS IN A SANDY SEDIMENT FOR A UNIT POINT SOURCE AT A HEIGHT ABOVE BOTTOM OF 100 m OPERATING AT 100 Hz

ARL-UT
AS-89-12
NPC-RFO
1-20-89

region of near-vertical contours that are widely spaced. In between, there is a region in which the contours change direction and form closed loops around periodic nulls. These three regions correspond to the refraction, evanescent, and interference zones indicated in Fig. 4.2. The periodic nulls are the result of interference between the evanescent and refracted waves. The spacing between the nulls is equal to the spatial period of the interference pattern.

Another example was computed for an acoustic frequency of 50 Hz, as shown in Fig. 4.4. It shows a similar pressure distribution, but the spatial period of the interference nulls are twice that of the 100 Hz case.

The above pressure contours were computed using the complex ray model, which assumes a fluid-fluid medium. The complex ray model is a very efficient algorithm, and therefore it is useful for obtaining qualitative estimates of the sound field. For quantitative analysis, we use the SAFARI model, which is a full wave solution for viscoelastic solid and liquid media. From the contours in Figs. 4.3 and 4.4, it is seen that the most interesting region appears to be beyond a range of 300 m and above a depth of 50 m. Therefore, to conserve computer resources, subsequent computations were confined to this region.

The pressure fields, as calculated by the SAFARI model for a point source 100 m above the interface projecting a 100 Hz acoustic wave, are shown in Figs. 4.5 and 4.6 for the silt and sand sediments. These contours should be compared with the pressure contours for the case of no sediment at all, shown in Fig. 4.7.

It is seen that the propagation loss in the silty sediment is not significantly different from that of the no-sediment case up to a range of about 900 m. Beyond this range, the effects of the critical angle in the sediment become apparent. There is an interference zone corresponding to the one illustrated in Fig. 4.1, in which there are significant pressure minima and maxima.

The pressure in the sand sediment computed by the SAFARI model appears to be similar in character to that produced by the complex ray model shown in Fig. 4.3, and the illustration in Fig. 4.2, showing the evanescent, refraction, and interference zones. At a more detailed level, the SAFARI model

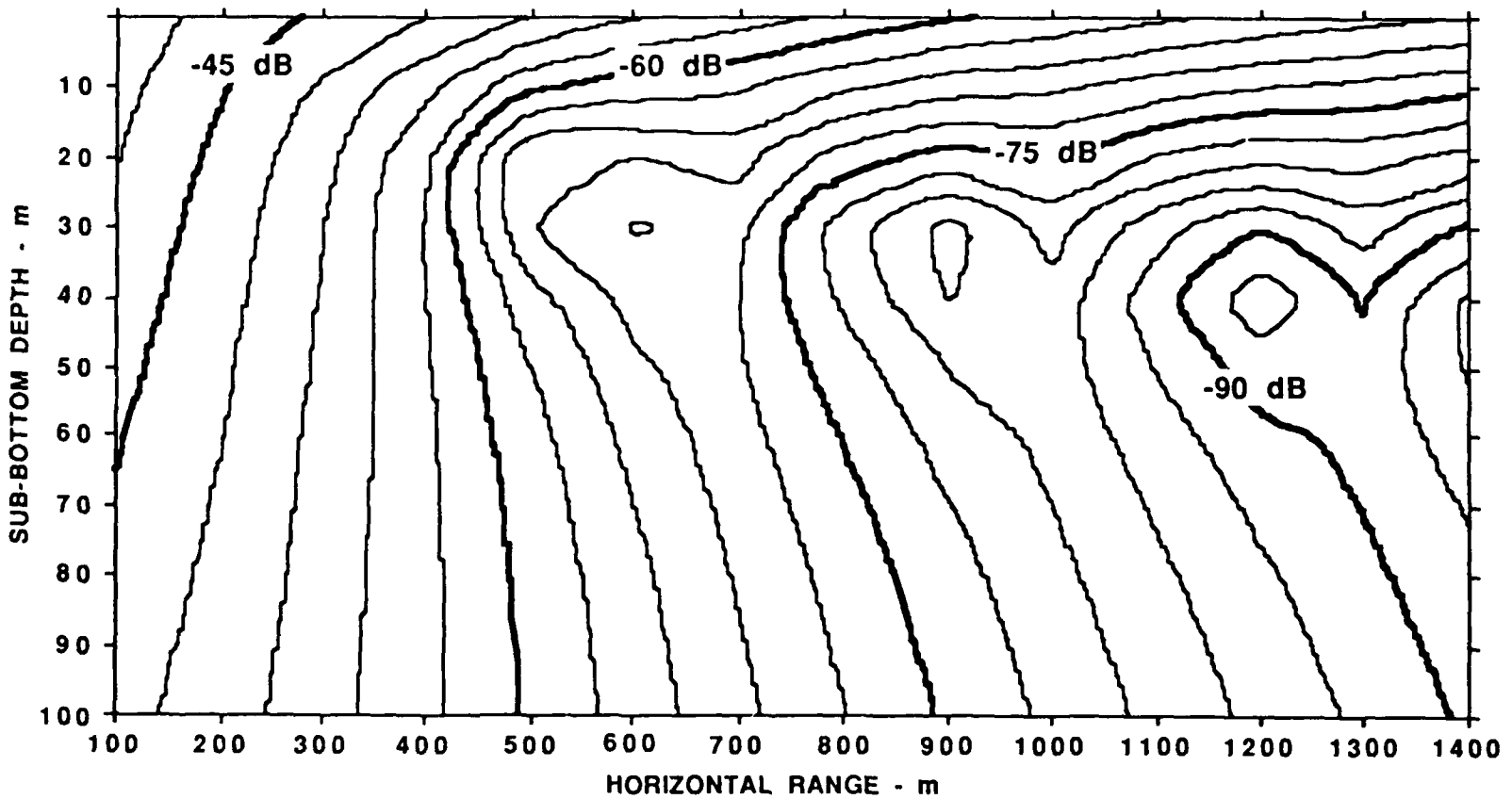

FIGURE 4.4
APPROXIMATE PRESSURE CONTOURS IN A UNIFORM SANDY SEDIMENT FOR A UNIT POINT SOURCE AT A HEIGHT ABOVE BOTTOM OF 100 m OPERATING AT 50 Hz

ARL-UT
AS-89-13
NPC-RFO
1-20-89

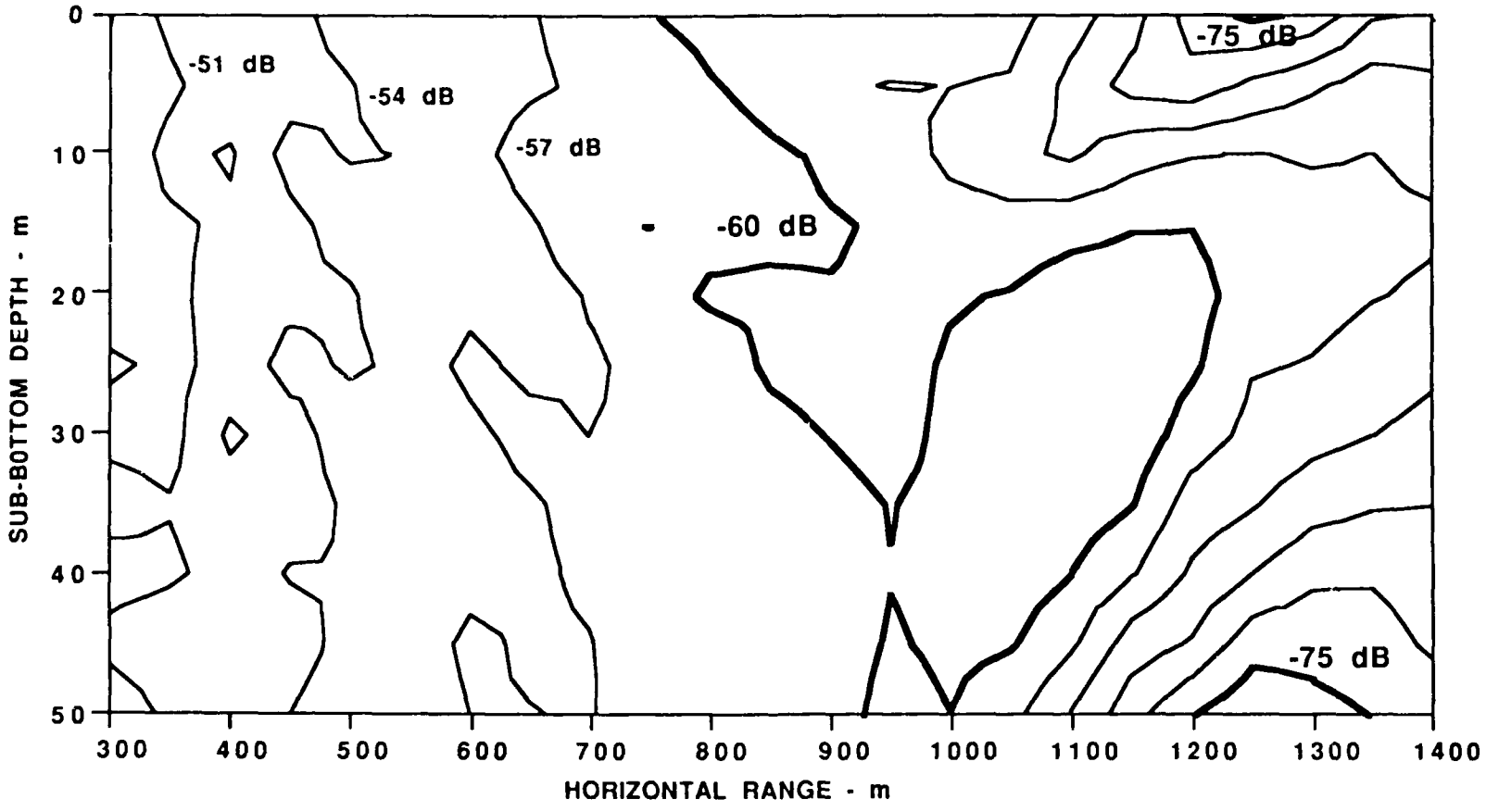

FIGURE 4.5
ACOUSTIC PRESSURE CONTOURS IN A SILTY SEDIMENT
COMPUTED BY THE SAFARI PROGRAM
FOR A UNIT POINT SOURCE AT A HEIGHT ABOVE BOTTOM OF 100 m
OPERATING AT 100 Hz

ARL-UT
AS-89-14
NPC-RFO
1-20-89

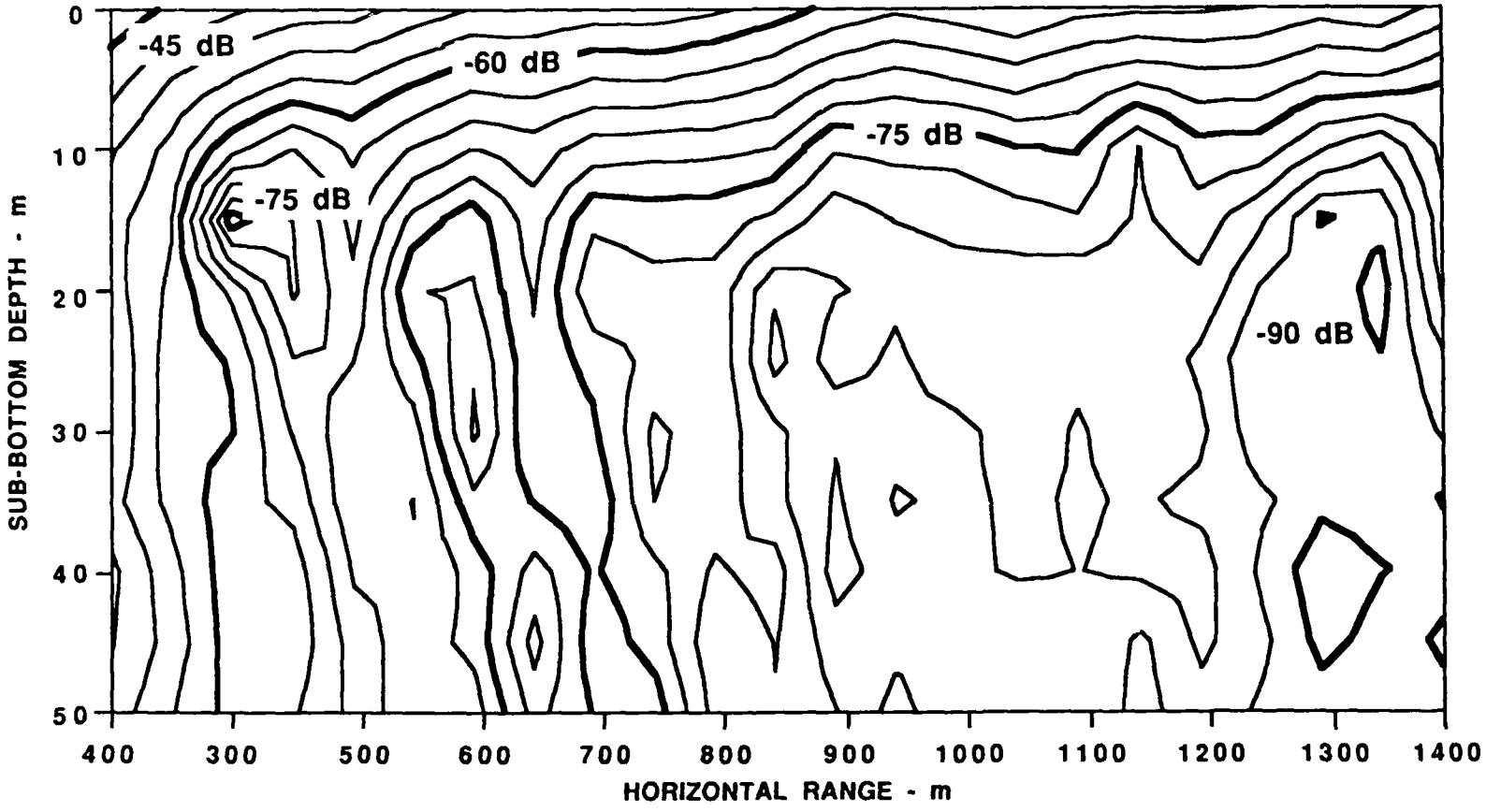

FIGURE 4.6
ACOUSTIC PRESSURE CONTOURS IN A SANDY SEDIMENT
COMPUTED BY THE SAFARI PROGRAM
FOR A UNIT POINT SOURCE AT A HEIGHT ABOVE BOTTOM OF 100 m
OPERATING AT 100 Hz

ARL - UT
AS-89-15
NPC - RFO
1 - 20 - 89

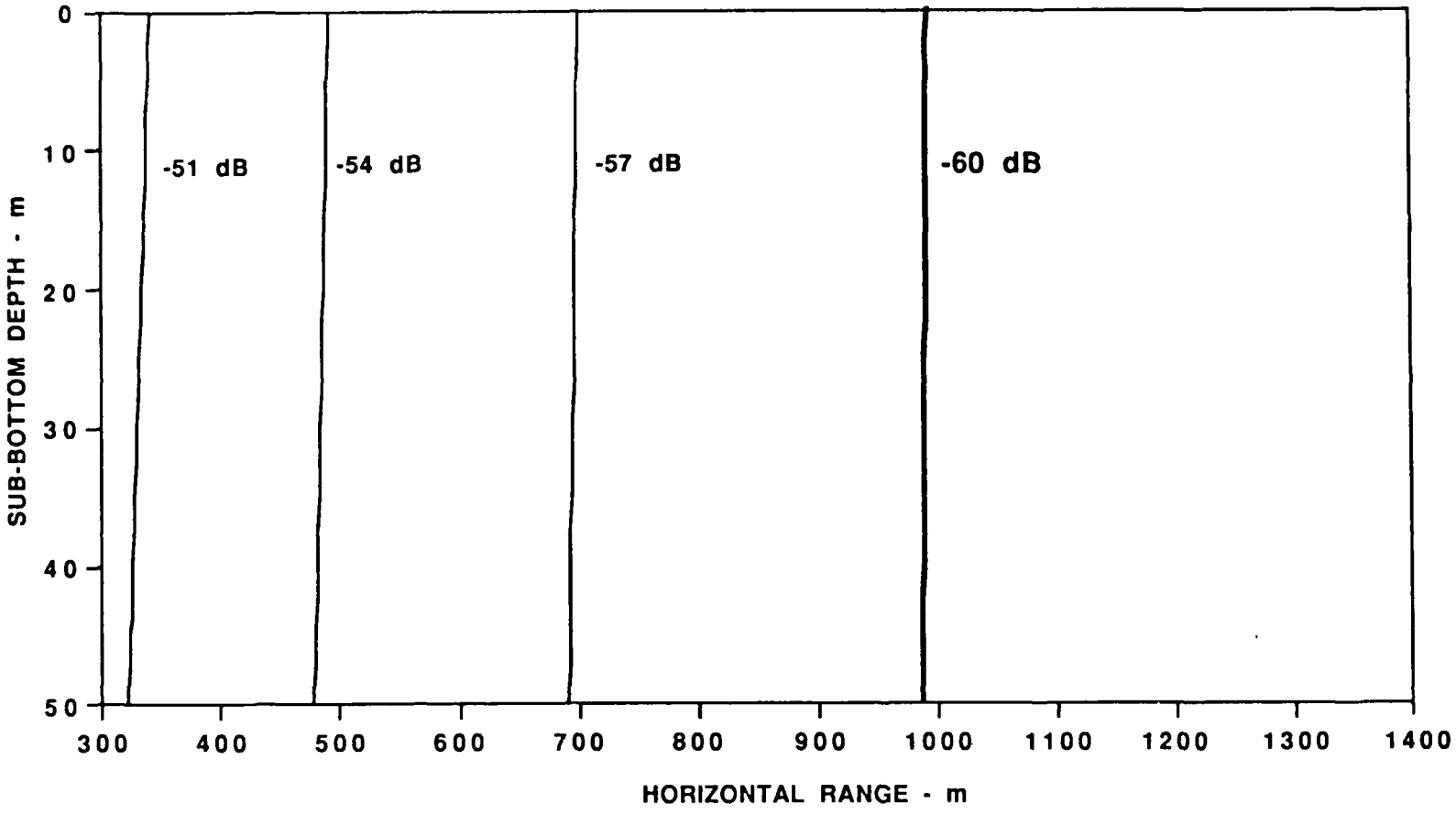

FIGURE 4.7
ACOUSTIC PRESSURE CONTOURS IN THE ABSENCE OF SEDIMENT
FOR A UNIT POINT SOURCE AT A HEIGHT OF 100 m
OPERATING AT 100 Hz

ARL - UT
AS-89-16
NPC - RFO
1 - 20 - 89

appears to give a more complicated pressure field than the complex ray model. This is not altogether surprising since there are significant differences between the two models; the main shortcoming of the complex ray model is that it is only a fluid-fluid model. A discussion of the differences and their reasons are beyond the scope of this report.

4.3 SEDIMENT FACTOR

Let us now consider a sonar with a widebeam projector that could be approximated by a point source, and a similar widebeam hydrophone.

Since a unit source was used, the inverse of the pressure contours in Figs. 4.5 and 4.6 may be directly equated to the forward propagation loss L_{r+}. Using Eqs. (3-7) and (3-8), the loss terms L_{r-} and L_z were estimated. Substituting into Eq. (2-5), the total propagation loss L_{2r} was estimated. Finally, substituting into Eq. (2-4), the sediment factor F_s was computed. The results for the silt and sand sediments are shown in Figs. 4.8 and 4.9.

In Fig. 4.8, it is seen that the sediment factor in the silty sediment is quite small for ranges up to 1000 m. Beyond this range, the interference effects due to the critical angle in the sediment begin to significantly distort the field, producing a patch of gain greater than 5 dB at a range of 1100 m and a depth of 25 m, and then giving way to increasing losses at longer ranges.

The sediment factor contours in the sand sediment, shown in Fig. 4.9, follow the same trends as the one-way propagation loss contours shown in Fig. 4.6. The refracted, evanescent, and interference zones are clearly visible. At 100 Hz, the acoustic wavelength is approximately 17 m. In the evanescent zone, it is seen that the sediment factor drops to a value less than -30 dB at a depth of one wavelength. The -30 dB contour appears to coincide with the boundary between the distinct zones. Beyond a range of 400 m, the -30 dB contour marks the boundary between the evanescent wave zone and the interference zone. Below a depth of approximately one wavelength, it marks the division between the refraction zone and the interference zone.

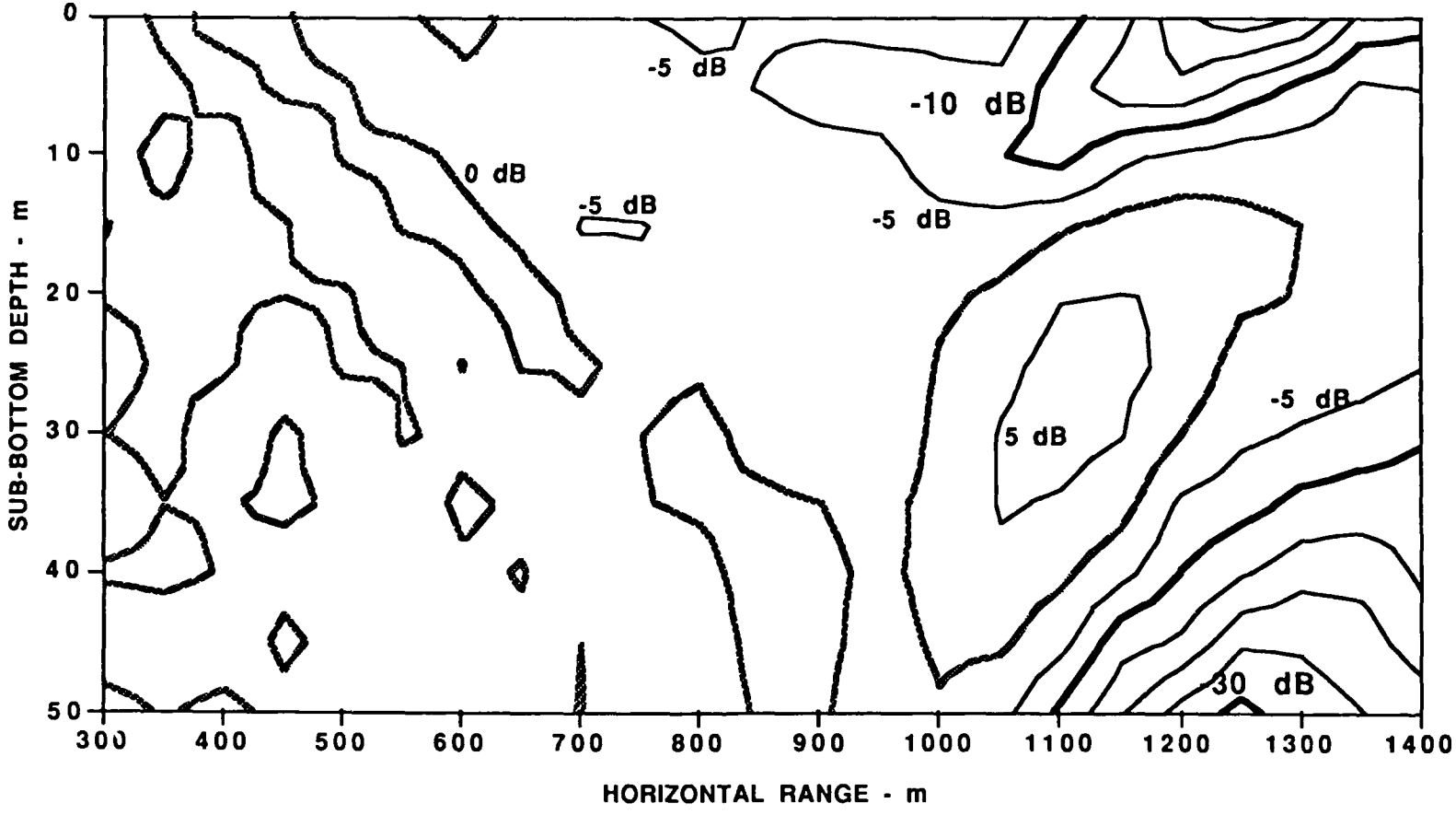

FIGURE 4.8
THE SEDIMENT FACTOR OF A SILTY SEDIMENT FOR A WIDEBEAM SONAR AT A HEIGHT OF 100 m OPERATING AT 100 Hz

ARL - UT
AS-89-17
NPC - RFO
1 - 20 - 89

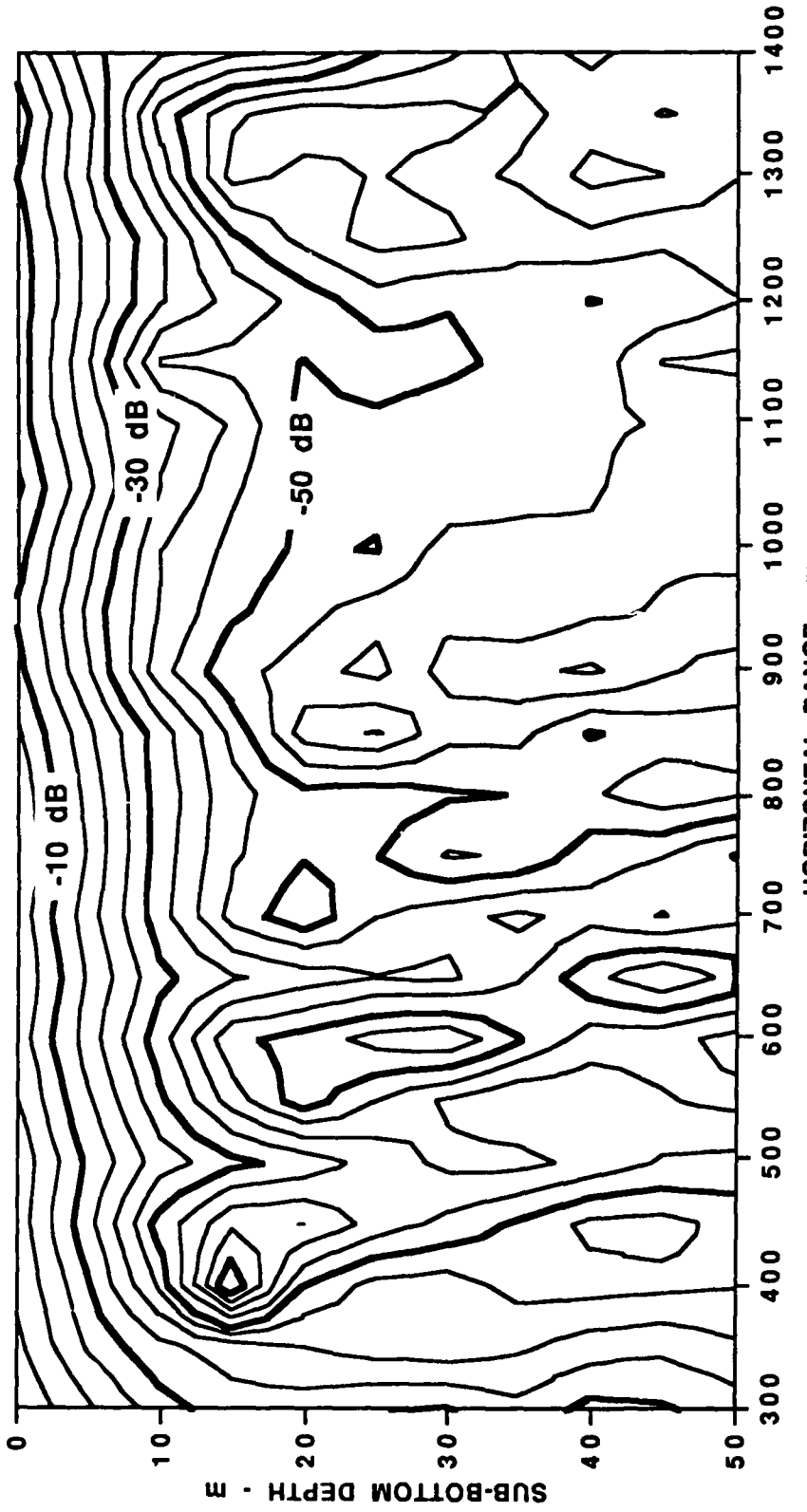

FIGURE 4.9
THE SEDIMENT FACTOR OF A SANDY SEDIMENT FOR A WIDEBEAM SONAR AT A HEIGHT OF 100 m OPERATING AT 100 Hz

ARL - UT
AS-89-18
NPC - RFO
1 - 20 - 89

The sediment factor contours may be plotted in a dimensionless space that will allow them to be applied to a broader range of operating conditions than the specific ones modeled here. We could have chosen three dimensionless parameters; that is, target depth, horizontal range, and sonar height in acoustic wavelengths. The first must be included because it determines the rate of decay of evanescent waves. The remaining two are not completely independent; it is expected that they may be replaced by a single parameter such as the incidence or grazing angle because of the strong influence the critical angle has on the acoustic field. We chose the grazing angle. The grazing angle, however, is difficult to define in a situation where ray paths are not clearly discernible. In the absence of a better definition, we have chosen to define the grazing angle as the inverse tangent of the sonar height divided by the horizontal range. The results are shown in Figs. 4.10 and 4.11. Although, strictly speaking, these plots will change with the operating frequency and sonar height above bottom, the dependence is expected to be weak, particularly outside the interference zones. Therefore, these plots are expected to be a useful representation of the behavior of small buried targets in general.

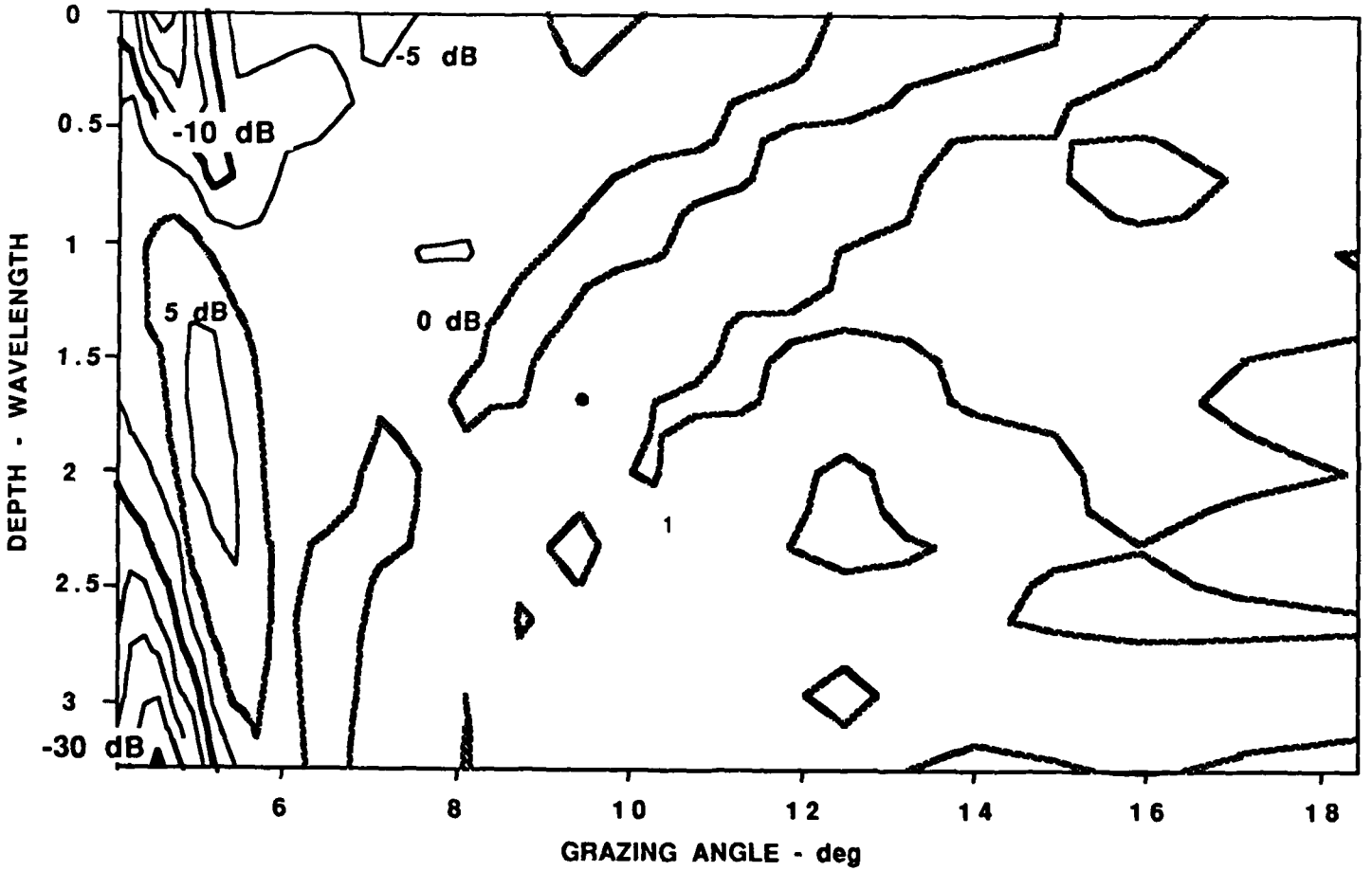

FIGURE 4.10
A DIMENSIONLESS PLOT OF THE SEDIMENT FACTOR OF A SILTY SEDIMENT FOR A WIDEBEAM SONAR AT A HEIGHT OF 100 m OPERATING AT 100 Hz

ARL - UT
AS-89-19
NPC - RFO
1 - 23 - 89

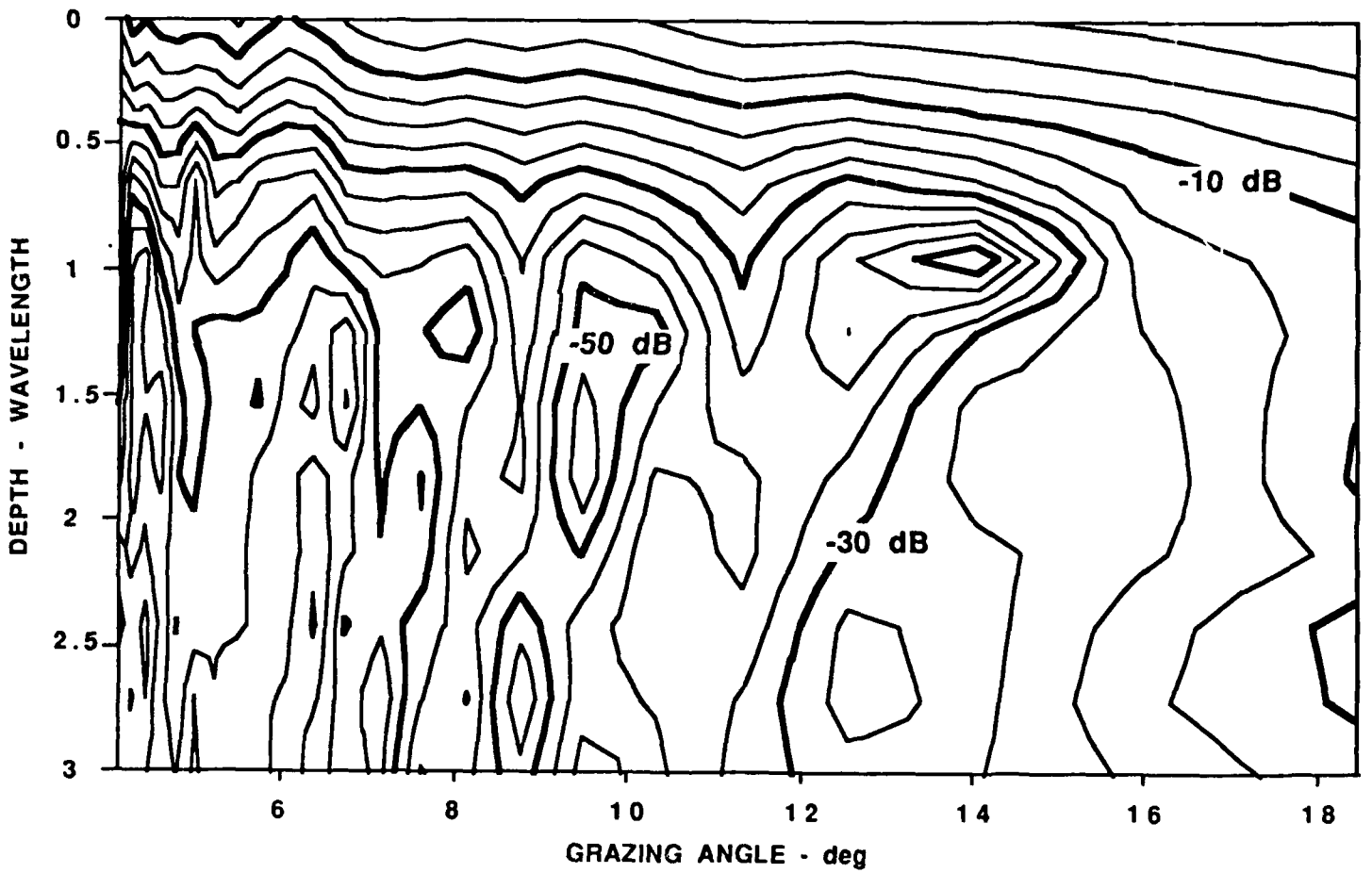

FIGURE 4.11
A DIMENSIONLESS PLOT OF THE SEDIMENT FACTOR OF A SANDY SEDIMENT FOR A WIDEBEAM SONAR AT A HEIGHT OF 100 m OPERATING AT 100 Hz

ARL-UT
AS-89-20
NPC-RFO
1-23-89

5. RESULTS AND CONCLUSIONS

We have looked at the behavior of a small target in two representative sediment types, a soft silty sediment whose sound velocity is slightly less than that of water and a sandy sediment with a much higher sound velocity. The reduction in the target echo due to the presence of the sediment was quantified as a "sediment factor". Specifically, the sediment factor was examined both qualitatively and quantitatively. Qualitatively, it was found that in both cases, the sound field in the sediment may be divided into distinct zones; in the silty sediment case, they are the refraction, critical, and interference zones, and in the sand sediment case, they are the refraction, evanescent, and interference zones. For quantitative results, computer simulations, using the SAFARI full wave mathematical model, were used to obtain numerical estimates of the sediment factor for a widebeam sonar at a height above bottom of 100 m and operating at 100 Hz. In a silty sediment, the sediment factor was near 0 dB in the refraction zone; beyond the refraction zone, the sediment factor varied about a declining mean due to the critical angle and interference effects. In the sand sediment, the sediment factor in the refraction zone was mainly caused by the absorption coefficient of the sediment; in the evanescent wave zone the sediment factor declined with increasing depth, reaching -30 dB at a depth of only one wavelength; in the interference zone, the sediment factor varied periodically, due to the interference between the refracted and evanescent waves, about a mean value of around –50 dB. Dimensionless plots of the sediment factor as a function depth in wavelengths and grazing angle in degrees were also obtained. These plots are believed to give a useful representation of the behavior of small buried targets in general. The sediment factor due to the presence of the sediment was found to be more complicated than expected. The results obtained in this report are based entirely on computer models and they remain to be verified by an experiment.

REFERENCES

1. M. A. Biot, "Mechanics of Deformation and Acoustics Propagation in Porous Media," J. Appl. Phys. 33, 1482-1498 (1962).

2. M. A. Biot, "Generalized Theory of Acoustic Propagation in Porous Dissipative Media," J. Acoust. Soc. Am. 34, 1254-1264 (1962).

3. M. A. Biot and D. G. Willis, "The Elastic Coefficients of the Theory of Consolidation," J. Appl. Mech. 24, 594-601 (1957).

4. M. A. Biot, "Theory of Propagation of Elastic Waves in a Fluid-Saturated Porous Solid -- I. Low Frequency Range," J. Acoust. Soc. Am. 28, 168-178 (1956).

5. M. A. Biot, "Theory of Propagation of Elastic Waves in a Fluid-Saturated Porous Solid -- II. Higher Frequency Range," J. Acoust. Soc. Am. 28, 179-191 (1956).

6. M. Stern, A. Bedford, and H. R. Millwater, "Wave Reflection from a Sediment Layer with Depth Dependent Properties," J. Acoust. Soc. Am. 77, 1781-1788 (1985).

7. A. N. Norris, "Radiation from a Point Source and Scattering Theory in a Fluid-Saturated Porous Solid," J. Acoust. Soc. Am. 77, 2012-2023 (1985).

8. R. A. Stephen, "A Comparison of Finite Difference and Reflectivity Seismograms for Marine Models," Geophys. J. R. Astr. Soc. 72, 39-58 (1983).

9. O. C. Zienkiewitz, The Finite Element Method, 3rd ed. (McGraw-Hill Book Co., Inc., London, 1977).

10. F. D. Tappert, "The Parabolic Approximation," in Wave Propagation and Underwater Acoustics, edited by J. B. Keller and J. S. Papadakis (Springer Verlag, Berlin, 1977), pp. 224-287.

11. M. W. Lawrence, "Ray Theory Modeling Applied to Low-Frequency Acoustic Interaction with Horizontally Stratified Ocean Bottoms," J. Acoust. Soc. Am. 78(2), 649-658 (1972).

12. F. B. Jensen and M. C. Ferla, "SNAP: The SACLANTCEN Normal-Mode Acoustic Propagation Model," SACLANTCEN Rep. SM-121, La Spezia, Italy, 1979.

13. H. Schmidt and F. B Jensen, "A Full Wave Solution for Propagation in Multilayered Viscoelastic Media with Application to Gaussian Beam Reflection at Fluid-Solid Interfaces," J. Acoust. Soc. Am. 77, 813-825 (1985).

14. R. B. Evans, "A Coupled Model Solution for Acoustic Propagation in a Waveguide with Stepwise Depth Variations of a Penetrable Bottom," J. Acoust. Soc. Am. 74, 188-195 (1983).

15. L. Satkowiak, private communication.

16. W. S. Rayleigh, The Theory of Sound, 2nd ed. (Dover, New York, 1955).

17. V. C. Anderson, "Sound Scattering from a Fluid Sphere," J. Acoust. Soc. Am. 22(4), 426-431 (1950).

18. R. J. Urick, Principles of Underwater Sound, 2nd ed. (McGraw-Hill Book Co., Inc., New York, 1975), p. 276.

19. E. L. Hamilton, "Attenuation of Shear Waves in Marine Sediments," J. Acoust. Soc. Am. 60(2), 334 (1976).

20. E. L. Hamilton, "Elastic Properties of Marine Sediments," J. Geophys. Res. 76, 579-604 (1971).

21. E. L. Hamilton, "Prediction of in situ Acoustic and Elastic Properties of Marine Sediments," Geophys. 36, 266-284 (1971).

22. E. L. Hamilton, "Compressional Wave Attenuation in Marine Sediments," Geophys. 37, 620-646 (1972).

23. E. L. Hamilton, "Geoacoustic Models of the Sea Floor," in Physics of Sound in Marine Sediments, edited by L. D. Hampton (Plenum Press, New York, 1974), pp. 181-221.

10 January 1989

DISTRIBUTION LIST FOR
ARL-TR-89-2
UNDER CONTRACT N00014-84-K-0082

Copy No.	
	Office of the Chief of Naval Research Department of the Navy Arlington, VA 22217-5000
1	Attn: R. Jacobson (Code 1125GG)
2	R. F. Obrochta (Code 1125AR, 1121)
3	CAPT. T. Brady (Code 122)
	Office of the Chief of Naval Research Office of Naval Technology Department of the Navy Arlington, VA 22217-5000
4	Attn: J. T. Warfield (Code 234)
	Commanding Officer Naval Ocean Research and Development Activity Stennis Space Center, MS 39529-5004
5	Attn: J. Matthews (Code 222)
6	P. Valent (Code 363)
7	Library
	Commanding Officer Office of Naval Research Detachment Stennis Space Center, MS 39529-5004
8	Attn: E. D. Chaika (Code 125)
9	B. Blumenthal (Code 125)
	Commanding Officer Naval Oceanographic Office Stennis Space Center, MS 39522-5001
10	Attn: W. Jobst (Code 7300)
11	R. Hecht (Code 7310)
12	Library
	Commander Space and Naval Warfare Systems Command Department of the Navy Washington, D.C. 20363-5100
13	Attn: R. Mitnick (PMW180-5)
14	D. Doolittle (PMW180-4)

Distribution list for ARL-TR-89-2 under Contract N00014-84-K-0082 (cont'd)

Copy No.	
	Director Naval Research Laboratory Washington, D.C. 20375
15	Attn: O. Diachok (Code 5120)
16	F. Ingenito (Code 5160)
17	D. Bradley (Code 5100)
18	W. Kuperman (Code 220)
19	Library
	Commanding Officer Naval Ocean Systems Center San Diego, CA 92152
20	Attn: H. Bucker (Code 541)
21	Library
	Office of the Chief of Naval Operations U. S. Naval Observatory 34th and Massachusetts Avenue Washington, D.C. 20390
22	Attn: CDR R. Hillyer (Code 006D3)
	Officer in Charge Naval Surface Warfare Center White Oak Laboratory Silver Spring, MD 20910
23 - 25	Attn: E. Hein (Code U21)
26	Library
	Commanding Officer David Taylor Research Center Bethesda, MD 20084
27	Attn: Library
	Commanding Officer Naval Air Development Center Warminster, PA 18974
28	Attn: L. Allen (Code 5033)
29	B. Steinberg (Code 5031)
30	Library

Distribution list for ARL-TR-89-2 under Contract N00014-84-K-0082 (cont'd)

Copy No.	
	Officer in Charge Naval Underwater Systems Center New London Laboratory New London, CT 06320
31	Attn: R. Deavenport (Code 3332)
32	W. Carey (Code 33A)
33	B. Cole (Code 33A)
34	Library
	Commander Naval Sea Systems Command Department of the Navy Washington, D.C. 20362-5101
35	Attn: Y. Yam (Code 63D4)
	Commander Naval Air Systems Command Department of the Navy Washington, D.C. 20360
36	Attn: W. Parigian (Code 933B)
37	Commanding Officer Naval Intelligence Support Center 4301 Suitland Road Washington, D.C. 20390
38 - 51	Commanding Officer and Director Defense Technical Information Center Cameron Station, Building 5 5010 Duke Street Alexandria, VA 22314
	Woods Hole Oceanographic Institution 86-95 Water Street Woods Hole, MA 02543
52	Attn: J. Lynch
53	G. Frisk
	Science Applications, Inc. 1710 Goodridge Drive McLean, VA 22101
54	Attn: P. Vidmar

Distribution list for ARL-TR-89-2 under Contract N00014-84-K-0082 (cont'd)

Copy No.

Applied Research Laboratory
The Pennsylvania State University
P.O. Box 30
State College, PA 16801

55 Attn: S. McDaniel
56 Library

Applied Physics Laboratory
The University of Washington
1013 N.E. 40 Street
Seattle, WA 98105

57 Attn: D. Jackson
58 Library

Scripps Institution of Oceanography
The University of California, San Diego
La Jolla, CA 92037

59 Attn: J. Orcutt

60 Hollis Boehme, ARL:UT

61 Nicholas P. Chotiros, ARL:UT

62 John M. Huckabay, ARL:UT

63 R. Stewart, ARL:UT

64 Library, ARL:UT

65 - 75 Reserve, ARL:UT